Inorg. Chem. **2007**, *46*, 8603–8612

Trinuclear Platinum(II) 4,6-Diphenyl-2,2′-bipyridyl Complex with Bis(diphenylphosphinomethyl)phenylphosphine Auxiliary Ligand: Synthesis, Structural Characterization, and Photophysics

Pin Shao and Wenfang Sun*

Department of Chemistry and Molecular Biology, North Dakota State University, Fargo, North Dakota 58105-5516

Received April 20, 2007

A trinuclear cyclometalated Pt(II) 4,6-diphenyl-2,2′-bipyridyl complex with bis(diphenylphosphinomethyl)-phenylphosphine bridging ligand ([**4-Ph(C^N^N)Pt]$_3$dpmp**) has been synthesized and characterized. It exhibits a broad electronic absorption band from 400 to 600 nm because of its intramolecular Pt···Pt interactions that have been revealed by X-ray crystal structure analysis. This complex shows strong red emission in acetonitrile at room temperature and 77 K. The electronic and emission spectra exhibit concentration and temperature dependence. With increased concentrations, the UV band of the absorption spectrum gradually decreases and broadens, accompanied by an increase of the ^{1}[dσ*,π*] band between 400 and 600 nm. For emission spectra, the 550 nm band that originates from the mononuclear platinum(II) component gradually decreases with increased concentrations, while the band at ∼700 nm that corresponds to the ^{3}[dσ*,π*] state increases. In addition, the UV–vis and emission spectra exhibit temperature and viscosity-dependence. The concentration-, temperature-, and viscosity-dependent characteristics indicate a conformational change of the complex arising from the rotation along the oligophosphine axis. This complex exhibits broad, positive, and strong transient difference absorption bands from the near-UV to near-IR spectral region. However, because of the increased ground-state absorption in the visible region, the nonlinear transmission of this trinuclear platinum complex decreases.

Introduction

Platinum(II) complexes with cyclometalating ligands have attracted increasing interest in recent years because of their potential applications in organic light-emitting devices,[1] chemical catalysis,[2] and chemical sensors.[3] Most of these complexes exhibit a square-planar configuration and show relatively strong emissions in visible spectral range at room temperature in fluids.[4] Because of the heavy metal effect of platinum, the intersystem-crossing rate of these complexes is generally high, which leads to a high quantum yield of the triplet excited state. In addition, many of the platinum terdentate complexes possess long-lived triplet excited states[5] and broad and relatively strong triplet transient difference absorption spectra.[6] These characteristics could result in

* To whom correspondence should be addressed. E-mail: Wenfang.Sun@ndsu.edu. Phone: 701-231-6254. Fax: 701-231-8831.

(1) (a) Lu, W.; Mi, B. X.; Chan, M. C. W.; Hui, Z.; Che, C. M.; Zhu, N.; Lee, S. T. *J. Am. Chem. Soc.* **2004**, *126*, 4958. (b) Yesin, H.; Donges, D.; Humbs, W.; Strasser, J.; Sitters, R.; Glasbeek, M. *Inorg. Chem.* **2002**, *41*, 4915. (c) Brooks, J.; Babayan, Y.; Lamansky, S.; Djurovich, P. I.; Tsyba, I.; Bau, R.; Thompson, M. E. *Inorg. Chem.* **2002**, *41*, 3055. (d) Shi, J. C.; Chao, H. Y.; Fu, W. F.; Peng, S. M.; Che, C. M. *J. Chem. Soc., Dalton Trans.* **2000**, *18*, 3128. (e) Chassot, L.; von Zelewsky, A.; Sandrini, D.; Maestri, M.; Balzani, V. *J. Am. Chem. Soc.* **1986**, *108*, 6084. (f) Maestri, M.; Sandrini, D.; Balzani, V.; Chassot, L.; Jolliet, P.; von Zelewsky, A. *Chem. Phys. Lett.* **1985**, *122*, 375. (g) Wong, W.-Y.; He, Z.; So, S.-K.; Tong, K.-L.; Lin, Z. *Organometallics* **2005**, *24*, 4079.

(2) (a) Dick, A. R.; Kampf, J. W.; Sanford, M. S. *Organometallics* **2005**, *24*, 482. (b) van der Boom, M. E.; Milstein, D. *Chem. Rev.* **2003**, *103*, 1759.

(3) (a) Yang, Q.-Z.; Wu, L.-Z.; Zhang, H.; Chen, B.; Wu, Z.-X.; Zhang, L.-P.; Tung, Z.-H. *Inorg. Chem.* **2004**, *43*, 5195. (b) Wu, L. Z.; Cheung, T. C.; Che, C. M.; Cheung, K. K.; Lam, M. H. W. *Chem. Commun.* **1998**, *10*, 1127. (c) Wong, K.-H.; Chan, M. C.-W.; Che, C. M. *Chem.—Eur. J.* **1999**, *5*, 2845. (d) Kui, S. C. F.; Chui, S. S.-Y.; Che, C.-M.; Zhu, N. *J. Am. Chem. Soc.* **2006**, *128*, 8297.

(4) (a) Lai, S.-W.; Chan, M. C. W.; Cheung, K.-K.; Peng, S.-M.; Che, C.-M. *Organometallics* **1999**, *18*, 3991. (b) Kwok, C.-C.; Ngai, H. M. Y.; Chan, S.-C.; Sham, I. H. T.; Che, C.-M.; Zhu, N. *Inorg. Chem.* **2005**, *44*, 4442. (c) Lai, S.-W.; Lam, H.-W.; Lu, W.; Cheung, K.-K.; Che, C.-M. *Organometallics* **2002**, *21*, 226. (d) Cheung, T.-C.; Cheung, K.-K.; Peng, S.-M.; Che, C. M. *J. Chem. Soc., Dalton Trans.* **1996**, 1645.

(5) (a) Yang, Q.-Z.; Wu, L.-Z.; Wu, Z.-X.; Zhang, L.-P.; Tung, C.-H. *Inorg. Chem.* **2002**, *41*, 5653. (b) Michalec, J. F.; Bejune, S. A.; Cuttell, D. G.; Summerton, G. C.; Gertenbach, J. A.; Field, J. S.; Haines, R. J.; McMillin, D. R. *Inorg. Chem.* **2001**, *40*, 2193.

10.1021/ic700757x CCC: $37.00
Published on Web 09/12/2007

strong reverse saturable absorption. Studies on the nonlinear optical properties of these complexes indicated that the platinum complexes could exhibit strong broadband nonlinear transmission.[6] Moreover, the photophysical properties and nonlinear transmission properties could be modulated by chemical modifications of coordination ligands.[5−7] It has also been reported in literature that the intermolecular metal−metal or $\pi-\pi$ interactions arising from aggregation in square planar Pt(II) complexes could influence the emission energy significantly.[8] Recent reports by Che's and others' groups on some binuclear and trinuclear Pt(II) complexes demonstrated that intramolecular Pt···Pt or $\pi-\pi$ interactions could occur in these multinuclear complexes, which modulates the energy of the excited states at some extent and leads to the appearance of a new metal−metal-to-ligand charge transfer (MMLCT or [dσ*, π*]) absorption band in the visible spectral range and a red-shift of the emission band.[9] Our group recently reported the effect of metal−metal coupling and $\pi-\pi$ interactions on the nonlinear transmission properties of three binuclear platinum(II) complexes.[6d] To further understand the effect of these interactions on the nonlinear transmission properties of multinuclear Pt(II) complexes, a new trinuclear cyclometalated Pt(II) 4,6-diphenyl-2,2′-bipyridyl complex ([**4-Ph(C^N^N)Pt]$_3$dpmp**, Figure 1) with bis(diphenylphosphinomethyl)phenylphosphine bridging ligand has been synthesized and characterized, and its photophysical characteristics and nonlinear transmission have been measured.

Experimental Section

Synthesis. The ligand bis(diphenylphosphinomethyl)phenylphosphine (dpmp) and the precursor complex 4,6-diphenyl-2,2′-bipyridyl platinum chloride ([4-Ph(C^N^N)Pt]Cl), were synthesized according to the reported procedures.[10] All the starting chemicals were purchased from Alfa Aesar. All the solvents were used as received unless otherwise stated.

^{1}H NMR spectra were measured on a Varian 500 MHz VNMR spectrometer. ESI-HRMS analyses were conducted on a Bruker Daltonics BioTOF III mass spectrometer. Elemental analyses were performed on a Perkin-Elmer 2400 Series II CHNS/O analyzer.

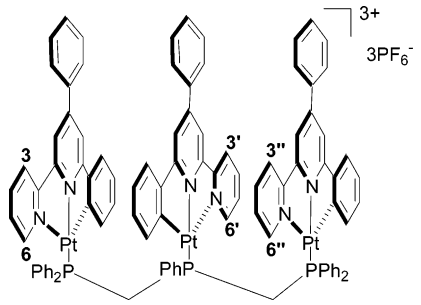

Figure 1. Chemical structure of **[4-Ph(C^N^N)Pt]$_3$dpmp**.

[4-Ph(C^N^N)Pt]$_3$dpmp. A mixture of 0.107 g (0.200 mmol) of 4-Ph(C^N^N)Pt]Cl and 0.037 g (0.067 mmol) of dpmp in 30 mL of CH_3CN/CH_3OH (1/1, v/v) was stirred for 24 h at room temperature under N_2 protection. The resultant clear solution was filtered into a saturated CH_3OH solution of NH_4PF_6. After removal of the solvent, the solid obtained was washed by water and ether. The crude product was recrystallized twice by diffusion of benzene into acetonitrile. Red crystals were obtained in 18% yield. ^{1}H NMR (CD_3CN): δ 8.01 (br, 4H), 7.92 (d, J = 8.0 Hz, 2H), 7.81 (t, J = 7.0 Hz, 4H), 7.70 (s, 2H), 7.63−7.66 (m, 6H), 7.51−7.57 (m, 10H), 7.25−7.49 (m, 34H), 7.11 (d, J = 7.5 Hz, 2H), 6.68 (t, J = 7.0 Hz, 4H), 6.61 (s, 2H), 6.46 (d, J = 7.0 Hz, 2H), 6.40 (t, J = 5.5 Hz, 1H), 6.32 (t, J = 7.5 Hz, 1H), 6.15 (t, J = 7.0 Hz, 2H), 5.37 (q, J = 11.5 Hz, 2H), 4.56 (q, J = 12.5 Hz, 2H) ppm. ESI-MS: m/z calcd for $[C_{98}H_{74}F_{12}N_6P_5{}^{195}Pt_3]^+$, 2302.3409; found, 2302.9835 (100%). Anal. Calcd for $C_{98}H_{74}F_{18}N_6P_6Pt_3\cdot C_6H_6$: C, 49.43; H, 3.19; N, 3.33. Found: C, 49.80; H, 2.70; N, 3.58.

Crystal Structure Determination. Single crystals of [**4-Ph(C^N^N)Pt]$_3$dpmp** were obtained by diffusion of benzene vapor into a dilute acetonitrile solution of the complex. A crystal with a dimension of 0.2 × 0.2 ×0.2 mm was sealed in a glass capillary with mother liquid. The capillary with crystal was transferred to a Bruker CCD diffractometer with graphite-monochromatized Mo Kα radiation (λ = 0.71073 Å). The frames were collected at ambient temperature with a scan width of 0.3° in ω and integrated with Bruker SAINT software package using narrow-frame integration algorithm. The unit cell was determined and refined by least-squares upon the refinement of *XYZ*-centeroids of reflections above 20σ(*I*). The data were corrected for absorption using SADABS program. The structures were refined on F^2 using the WinGx software package.[11] The crystal structure was solved by the direct method. All of the non-hydrogen atoms were refined with anisotropic displacement coefficients. Hydrogen atoms were idealized using SHELXL97.[12] The weighting scheme employed was $w = 1/[\sigma^2(F_o^2) + (0.1311)^2 + 24.6706P]$, where $P = (F_o^2 + 2F_c^2)/3$. The refinement converged to $R_1 = 0.0526$, $R_2 = 0.1343$ for reflections with $I > 2\sigma$ (I) and $R_1 = 0.1203$, $R_2 = 0.1506$ for all data. ($R_1 = \sum(||F_o| - |F_c||)/\sum|F_o|$, $R_2 = [\sum(w(F_o^2 - F_c^2)2)/\sum(F_o^2)^2]^{1/2}$, and S = GOF on $F^2 = [\sum(w(F_o^2 - F_c^2)^2/(n - p))]^{1/2}$, where n is the number of reflections and p is the number of parameters refined). Crystallographic and structural refinement data are listed in Table 1.

Results and Discussion

Crystal Structure. The crystal structure of the [**4-Ph(C^N^N)Pt]$_3$dpmp** cation is depicted in Figure 2. Selected

(6) (a) Sun, W.; Wu, Z.-X.; Yang, Q.-Z.; Wu, L.-Z.; Tung, C.-H. *Appl. Phys. Lett.* **2003**, *82*, 850. (b) Guo, F.; Sun, W.; Liu, Y.; Schanze, K. *Inorg. Chem.* **2005**, *44*, 4055. (c) Sun, W.; Guo, F. *Chin. Opt. Lett.* **2005**, *S3*, S34. (d) Sun, W.; Zhu, H.; Barron, P. M. *Chem. Mater.* **2006**, *18*, 2602.
(7) (a) Lu, W.; Mi, B.-X.; Chan, M. C. W.; Hui, Z.; Che, C.-M.; Zhu, N.; Lee, S.-T. *J. Am. Chem. Soc.* **2004**, *126*, 4958. (b) Farley, S. J.; Rochester, D. L.; Thompson, A. L.; Howard, J. A. K.; Williams, J. A. G. *Inorg. Chem.* **2005**, *44*, 9690. (c) Crites, D. K.; Cunningham, C. T.; McMillin, D. R. *Inorg. Chim. Acta* **1998**, *273*, 346.
(8) (a) Ma, B.; Li, J.; Djurovich, P. I.; Yousufuddin, M.; Bau, R.; Thompson, M. E. *J. Am. Chem. Soc.* **2005**, *127*, 28. (b) Lai, S.-W.; Chan, M. C.-W.; Cheung, T.-C.; Peng, S.-M.; Che, C.-M. *Inorg. Chem.* **1999**, *38*, 4046. (c) Lu, W.; Chan, M. C. W.; Cheung, K.-K.; Che, C.-M. *Organometallics* **2001**, *20*, 2477.
(9) (a) Lu, W.; Chan, M. C. W.; Zhu, N.; Che, C.-M.; Li, C.; Hui, Z. *J. Am. Chem. Soc.* **2004**, *126*, 7639. (b) Kui, S. C. F.; Sham, I. H. T.; Cheung, C. C. C.; Ma, C. W.; Yan, B. P.; Zhu, N. Y.; Che, C. M.; Fu, W. F. *Chem.—Eur. J.* **2007**, *13*, 417. (c) Kui, S. C. F.; Chui, S. S.-Y.; Che, C.-M.; Zhu, N. *J. Am. Chem. Soc.* **2006**, *128*, 8297. (d) Yam, V. W.-W.; Chan, K. H.-Y.; Wong, K. M.-C.; Chu, B. W.-K. *Angew. Chem., Int. Ed.* **2006**, *45*, 6169.
(10) (a) Appel, R.; Geisler, K.; Scholer, H. F. *Chem. Ber.* **1979**, *112*, 648. (b) Cheung, T.-C.; Cheung, K.-K.; Peng, S.-M.; Che, C. M. *J. Chem. Soc., Dalton Trans.* **1996**, 1645.
(11) Farrugia, L. J. *WinGX, A Windows Program for Crystal Structure Analysis*; University of Glasgow: Glasgow, U.K., 1998.
(12) Sheldrick, G. M. *SHELX97, Programs for Crystal Structure Analysis*, release 97-2; University of Göttingen: Göttingen, Germany, 1997.

Table 1. Crystallographic and Structural Refinement Data for **[4-Ph(C^N^N)Pt]$_3$dpmp**

empirical formula	$C_{115}H_{92}F_{18}N_7P_6Pt_3$
fw	2685.05
cryst syst	triclinic
space group	$P\bar{1}$
a (Å)	16.217(10)
b (Å)	19.452(10)
c (Å)	20.925(10)
α (deg)	69.59(10)
β (deg)	70.89(10)
γ (deg)	87.72(10)
V (Å^3)	5825(5)
Z	2
ρ_{calcd} (g cm^{-3})	1.531
μ (cm^{-1})	3.75
F(000)	2634
T (K)	293(2)
wavelength (Å)	0.71073
data collection range (deg)	1.97−26.50
index ranges	$-20 \le h \le 0$
	$-24 \le k \le 24$
	$-26 \le l \le 21$
no. of unique data	20 432
final [$I > 2\sigma(I)$][a]	R1 = 0.0526
	wR2 = 0.1343
R indices (all data)[a]	R1 = 0.1203,
	wR2 = 0.1506

[a] $R1 = \sum(||F_o| - |F_c||)/\sum|F_o|$, $wR2 = [\sum(w(F_o^2 - F_c^2)^2)/\sum(F_o^2)^2]^{1/2}$.

bond lengths and bond angles are listed in Table 2. The relevant bond angles around platinum(II) deviate from the ideal values of 90 or 180°, indicating that each platinum(II) metal center adopts a distorted square-planar geometry. The Pt−N, Pt−P, and Pt−C distances in the complex are similar to other 4,6-diphenyl-2,2′-bipyridyl-containing dinuclear or trinuclear platinum(II) complexes reported in the literature.[9a,9b,10b] The three [4-Ph(C^N^N)Pt]$^+$ moieties are arranged into a linear face-to-face configuration by the dpmp ligand. The Pt(1)−Pt(2)−Pt(3) angle is 168.5°, and the distances of the two neighboring Pt atoms are 3.469 Å between Pt(1) and Pt(2) and 3.168 (0.5) Å between Pt(2) and Pt(3). These values are comparable or slightly shorter than those of other trinuclear 4′-substituted C^N^N complexes reported in the literature, such as **[(C^N^N)$_3$Pt$_3$(μ_3-dpmp)](ClO$_4$)$_3$·H$_2$O** (3.194 and 3.399 Å),[9a] **[(C^N^N)$_3$Pt$_3$-(μ_3-dpmp)](ClO$_4$)$_3$·2Et$_2$O·CH$_3$CN** (3.364 and 3.617 Å),[9a] **[{4,4′-^{t}Bu$_2$(C^N^N)}$_3$Pt$_3$(μ-dpmp)](ClO$_4$)$_3$·3CH$_3$CN** (3.217 and 3.601 Å),[9a] **[{4-EtO$_2$C(C^N^N)}$_3$Pt$_3$(μ_3-dpmp)](ClO$_4$)$_3$·2CH$_3$CN** (3.466 and 3.647 Å),[9a] and **[{^{t}Bu(C^N^N)}$_3$Pt$_3$-(μ-dpmp)](ClO$_4$)$_3$·2CH$_3$CN** (3.300 and 3.533 Å).[9b] The distance between the two neighboring Pt atoms just falls in the range of effective metal−metal interaction distance (3.09−3.50 Å) that is usually observed in extended linear-chain-arranged monomeric Pt(II) structures.[13] Therefore, weak d^8···d^8 interactions exist across Pt(1)−Pt(2)−Pt(3), and the interaction between Pt(2) and Pt(3) is stronger than that of Pt(1)−Pt(2) because of the shorter distance. For the same reason, the Pt···Pt interactions in this complex are comparable or stronger than those in the aforementioned reported complexes. To reduce the repulsive forces introduced by the overlap of two neighboring ligated Pt(II) planes, the torsion

(13) Miskowski, V. M.; Houlding, V. H. *Inorg. Chem.* **1991**, *30*, 4446.

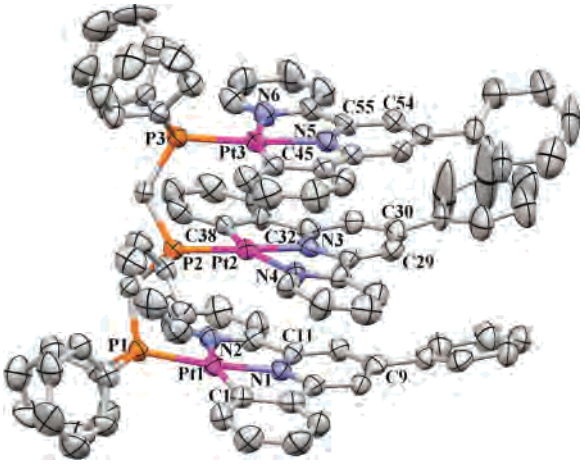

Figure 2. Perspective view of the complex cation of **[4-Ph(C^N^N)-Pt]$_3$dpmp** with selected atomic numbering scheme. The thermal ellipsoids are at 50% probability. All hydrogen atoms, solvent molecules (2.5 C_6H_6 and 1 CH_3CN), and counteranions ($3PF_6^-$) have been omitted for clarity.

Table 2. Selected Bond Lengths (Å) and Bond Angles (deg) for Complex Cation of **[4-Ph(C^N^N)Pt]$_3$dpmp**

Pt(1)−C(1)	2.005(9)	Pt(1)−N(1)	2.003(7)
Pt(1)−N(2)	2.156(8)	Pt(1)−P(1)	2.267(2)
Pt(2)−C(38)	2.033(9)	Pt(2)−N(3)	2.020(7)
Pt(2)−N(4)	2.174(8)	Pt(2)−P(2)	2.271(2)
Pt(3)−C(45)	2.034(1)	Pt(3)−N(5)	2.016(8)
Pt(3)−N(6)	2.140(8)	Pt(3)−P(3)	2.257(3)
C(1)−Pt(1)−N(1)	80.4(4)	C(1)−Pt(1)−N(2)	157.6(3)
C(1)−Pt(1)−P(1)	104.2(3)	N(1)−Pt(1)−N(2)	77.6(3)
N(1)−Pt(1)−P(1)	173.0(2)	N(2)−Pt(1)−P(1)	98.1(2)
C(38)−Pt(2)−N(3)	79.8(5)	C(38)−Pt(2)−N(4)	156.8(3)
C(38)−Pt(2)−P(2)	96.5(3)	N(3)−Pt(2)−N(4)	76.8(3)
N(3)−Pt(2)−P(2)	176.5(2)	N(4)−Pt(2)−P(2)	106.7(2)
C(45)−Pt(3)−N(5)	80.7(4)	C(45)−Pt(3)−N(6)	157.8(3)
C(45)−Pt(3)−P(3)	97.3(3)	N(5)−Pt(3)−N(6)	77.2(3)
N(5)−Pt(3)−P(3)	174.7(2)	N(6)−Pt(3)−P(3)	104.6(2)

angle between ligated Pt(1) plane and Pt(2) plane is smaller than the torsion angle between Pt(2) plane and Pt(3) plane: the torsion angles are 11.83 and 22.22° about Pt(1)−Pt(2) and Pt(2)−Pt(3) axes, respectively (defined by the angle between the N(1)−Pt(1)−Pt(2) and Pt(1)−Pt(2)−N(3) planes and that between the N(3)−Pt(2)−Pt(3) and Pt(2)−Pt(3)−N(5) planes). When the phenyl substituent at the cyclometalated ligand becomes more involved in the π-conjugation of the C^N^N ligand, the extent of slipping or offset between the ligand planes decreases. The C^N^NPt planes in the compound are almost parallel to each other with the dihedral angles between the planes N(1)−C(11) and N(3)−C(32) being 3.8° and that between the planes N(3)−C(32) and N(5)−C(55) being 2.4°. The shortest interplane atom···atom separations are 3.446 Å for C(9)···C(29) and 3.442 Å for C(30)···C(54). This makes the π···π interactions or C···π interactions feasible. Although these interactions are weak, they could be important in molecular assembly. It should also be noted that the introduction of a phenyl substituent at the 4-position of each C^N^N ligand only induces little steric hindrance. The phenyl ring is almost coplanar to the C^N^N plane with torsion angles of 19.9, 19.1, and 36.7° in Pt(1), Pt(2), and Pt(3) moieties, respectively.

Figure 3 displays a portion of the molecular-packing diagram. The shortest distance between two Pt atoms in

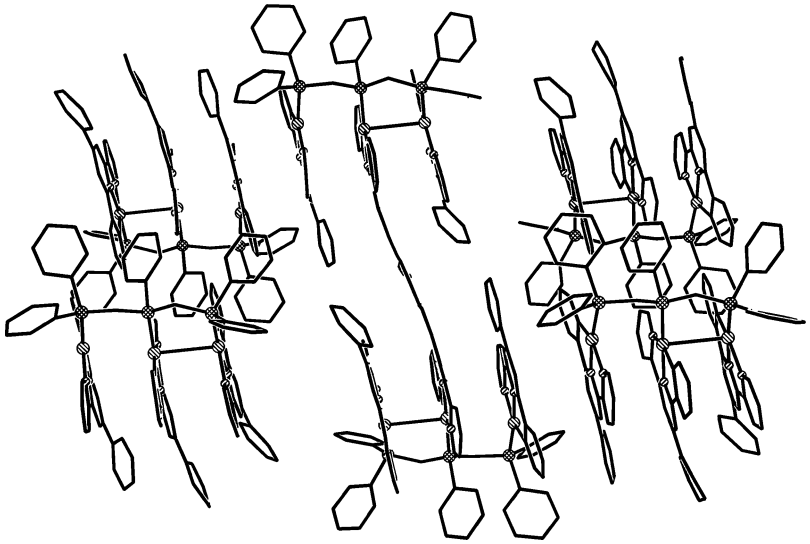

Figure 3. Portion of the molecular packing diagram of complex cation of **[4-Ph(C^N^N)Pt]$_3$dpmp.**

adjacent molecules is 7.612 Å; therefore, no intermolecular Pt···Pt interactions is possible even in the crystal form.

UV−vis Spectra. The UV−vis spectra of **[4-Ph(C^N^N)Pt]$_3$dpmp** are displayed in Figure 4. Like the trinuclear Pt(II) complexes reported,[9a] **[4-Ph(C^N^N)Pt]$_3$dpmp** also exhibits a broad and weak absorption band in the region of 450−600 nm, which can be attributed to the ^{1}[dσ*, π*], that is, the ^{1}MMLCT (metal−metal-to-ligand charge transfer) transition resulting from Pt···Pt interactions. The presence of intramolecular Pt···Pt interactions has been confirmed by the crystal structure of the **[4-Ph(C^N^N)Pt]$_3$dpmp** complex, in which the separation between the neighboring Pt metals is within the metal−metal coupling distance (3.09−3.50 Å). Interestingly, the UV−vis spectrum of **[4-Ph(C^N^N)Pt]$_3$dpmp** complex, especially the ^{1}[dσ*, π*] transition band, exhibits concentration-, temperature-, and solvent-dependence. As shown in Figure 4A, when the concentration of solution increases, the band at ∼280 nm decreases, along with a slight red shift. Meanwhile, the fine structures in the 300−400 nm region disappear, and the extinction coefficient of the low energy ^{1}[dσ*, π*] band increases. This indicates that the intramolecular Pt···Pt interactions increase with an increased concentration. Alternatively, these changes could be attributed to intermolecular interactions resulting from aggregation. However, attribution to intramolecular interaction is preferred because of the evidence from the crystal structure, which manifests that the three **4-Ph(C^N^N)Pt** components adopt a face-to-face geometry and the separation between neighboring Pt metals is within the metal−metal coupling distance (3.09−3.50 Å). In contrast, the shortest intermolecular metal−metal distance is found to be 7.612 Å; therefore, intermolecular metal−metal interaction is not possible even in the crystal form. Further evidence to exclude the intermolecular interactions has been found from the emission studies of SDS micell solutions, which will be discussed in the following emission section.

The observation of ^{1}[dσ*, π*] band at higher concentrations is obvious but not at dilute concentrations, which suggests that there could exist different conformers in solutions when concentration changes, as observed in the corresponding dinuclear platinum(II) complexes **[4-Ph(C^N^N)Pt]$_2$dppm** and **[4-Ph(C^N^N)Pt]$_2$dppe**.[6d] Such a conformation change could be induced by rotation of the 4-Ph(C^N^N)Pt components along the oligophosphine ligand. The rotation rate or degree of rotation are influenced by the concentration, temperature, and viscosity of the solution. At higher concentrations, the face-to-face *syn* conformer with feasible metal−metal interactions could dominate, resulting in the ^{1}[dσ*, π*] band. In contrast, at lower concentrations, the degree of rotation could become larger, which breaks down the metal−metal interactions and thus reduces the ^{1}[dσ*, π*] band intensity. Unfortunately, the reason that causes this concentration-dependent phenomenon still remains unclear at this time and needs to be investigated in the future.

The UV−vis spectrum also exhibits temperature dependence. As shown in Figure 4B, with increased temperatures, the intensity of the ^{1}[dσ*, π*] band decreases, indicating that the intramolecular Pt···Pt interactions decrease. This should be attributed to the increased rotation between the two neighboring ligated Pt moieties along the oligophosphine axis at higher temperatures, which causes the conformational change and destroys the intramolecular Pt···Pt interactions. The temperature-induced conformational change has also been reported by Yam and co-workers for three dinuclear platinum(II) terpyridyl complexes with appropriate flexible bridge and "sticky ends", although this change was described as intramolecular aggregation and deaggregation in their work.[9d] The hypothesis of rotation of ligated Pt moiety along the oligophosphine axis can be further supported by the emission study in solutions with different viscosity, which will be discussed in the emission section shortly.

The UV−vis absorption spectrum of **[4-Ph(C^N^N)Pt]$_3$dpmp** in different solvents is illustrated in Figure 4C and Table 3. It exhibits an insignificant solvatochromic effect, and no general trend has been observed. The ^{1}[dσ*, π*] band blue shifts in acetone and acetonitrile in comparison to those in DCM and THF. However, more polar solvents, such as

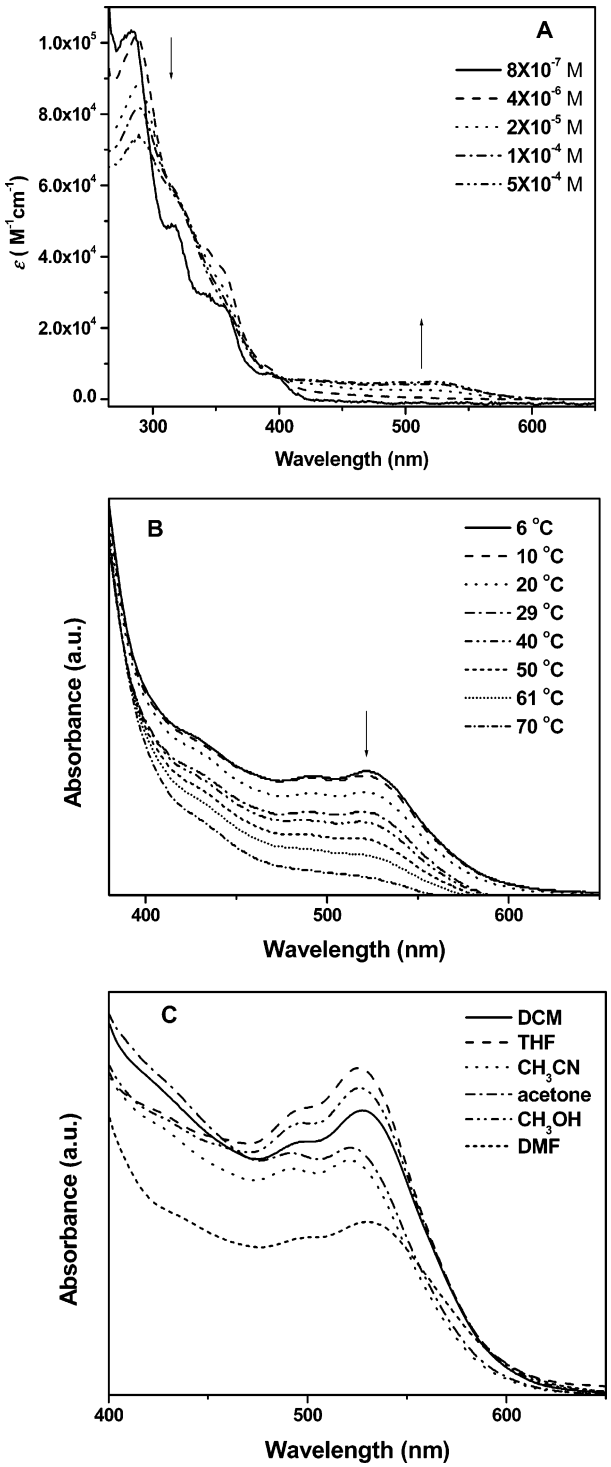

Figure 4. UV−vis spectra of **[4-Ph(C^N^N)Pt]$_3$dpmp** complex (A) in CH_3CN at different concentrations at room temperature, (B) in CH_3CN at different temperatures (solution concentration is 3.1×10^{-5} mol/L), and (C) in different solvents at room temperature (solution concentration is 1.2×10^{-4} mol/L).

DMF, cause a slight red shift of the ^{1}[dσ*, π*] band compared to those in DCM and THF.

Emission. [**4-Ph(C^N^N)Pt]$_3$dpmp** is emissive at room temperature in acetonitrile solution and at 77 K in acetonitrile glassy solution (Figure 5). At lower concentrations, the emission spectrum consists of two bands in CH_3CN at room temperature, one band is at ~700 nm and the other one is at

Table 3. UV−vis and Emission Band Maxima of **[4-Ph(C^N^N)Pt]$_3$dpmp** in Different Solvents at Room Temperature[a]

Solvent	λ_{abs} (nm)	λ_{em} (nm) (τ_{em} (ns))[b]	τ_{TA} (ns)[c]
THF	289, 321, 496, 526	697 (974)	901
DCM	290, 319, 496, 527	697 (1033)	891
Acetone	317, 492, 521	699 (718)	570
CH_3CN	288, 492, 521	699 (708)	578
MeOH	289, 319, 496, 526	712 (245)	229
DMF	289, 324, 499, 530	715	

[a] Measured at a concentration of 1.2×10^{-4} mol/L. [b] $\lambda_{ex} = 491$ nm. [c] Measured at 600 nm. $\lambda_{ex} = 355$ nm.

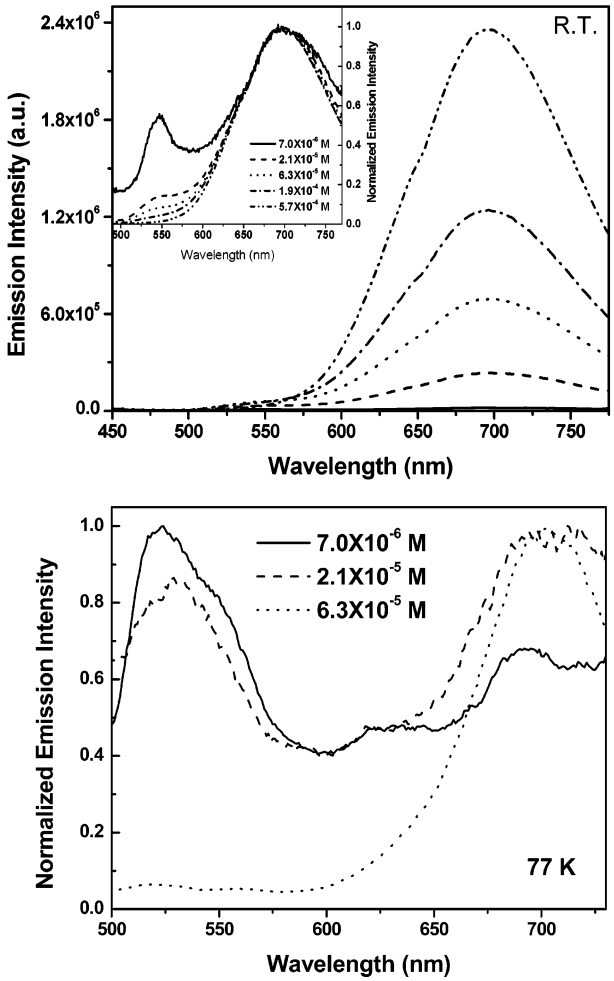

Figure 5. Concentration-dependent emission spectra of **[4-Ph(C^N^N)-Pt]$_3$dpmp** in acetonitrile at room temperature ($\lambda_{ex} = 400$ nm) and 77 K ($\lambda_{ex} = 380$ nm). The inset shown in the room-temperature emission figure is the corresponding normalized emission spectra.

~542 nm. With increased concentrations, the emission band at ~700 nm increases, while the intensity of the emission band at 542 nm decreases. Similar to the emission of other trinuclear platinum(II) complexes reported in the literature,[9a] the emission at ~700 nm can be attributed to the ^{3}[dσ*, π*], that is, ^{3}MMLCT state, whereas the high-energy emission band at 542 nm is ascribed to the ^{3}MLCT state in the 4-Ph-(C^N^N)Pt component when the molecule adopts a twisted conformation that exhibits no metal−metal interactions. As discussed in the UV−vis spectra, [**4-Ph(C^N^N)Pt]$_3$dpmp** exhibits a conformational transformation in solution caused by the rotation along the oligophosphine axis. At lower

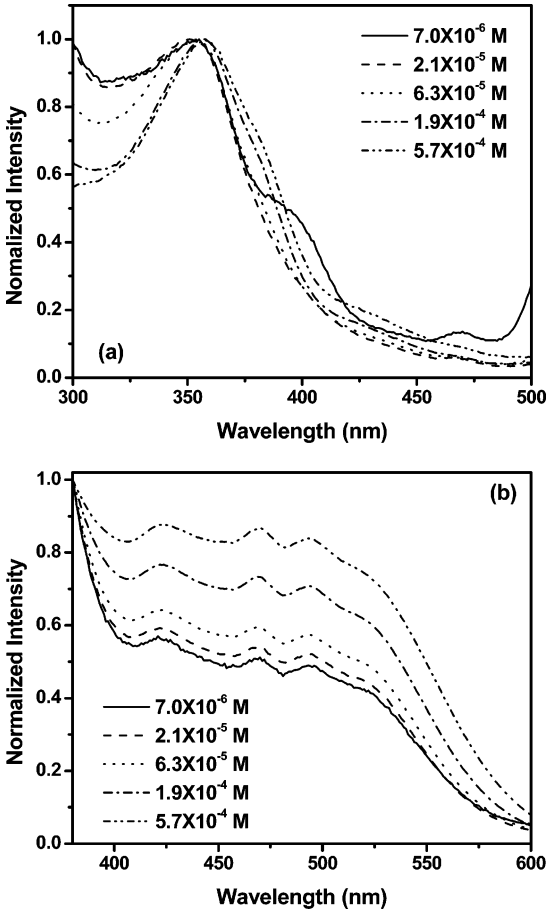

Figure 6. Normalized excitation spectra of **[4-Ph(C^N^N)Pt]$_3$dpmp** at different concentrations in CH_3CN at room temperature: (a) monitored at 545 nm and (b) 700 nm.

concentrations, the percentage of twisted conformer without intramolecular metal−metal coupling is higher. Thus, the emission originated from the ^{3}MLCT state of the mononuclear 4-Ph(C^N^N)Pt component is stronger. As the concentration of solution increases, the percentage of *syn* conformers increases. Because of the intramolecular Pt···Pt interactions in the *syn* conformers, the low-energy emission band corresponding to the $^3[d\sigma^*, \pi^*]$ state is enhanced. For low-temperature (77 K) emission, a similar trend has been observed.

To confirm the different origin of the two emission bands at lower concentrations, emission spectra at a different excitation wavelength ($\lambda_{ex} = 491$ nm for room-temperature emission and $\lambda_{ex} = 530$ nm for 77 K emission), where it is located in the $^1[d\sigma^*, \pi^*]$ band, have been measured. As shown in the Supporting Information (Figures S1 and S2), only the 700 nm band appears. This clearly indicates that the emission at ~700 nm arises from the $^3[d\sigma^*, \pi^*]$ excited state. Furthermore, the excitation spectra monitored at 545 and 700 nm exhibit different features (Figure 6). The excitation spectra monitored at 545 nm exhibit a strong band at ~350 nm, while the excitation spectra monitored at 700 nm show a broad band in the range of 400−600 nm, which is consistent with the $^1[d\sigma^*, \pi^*]$ transition band in the UV−vis spectra. Therefore, we conclude that the low-energy emission at ~700 nm arises from the $^3[d\sigma^*, \pi^*]$ excited state.

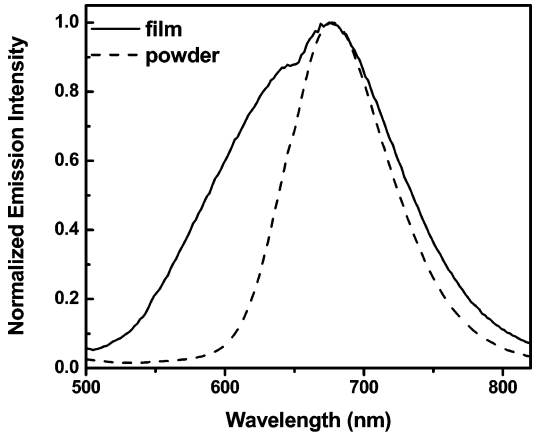

Figure 7. Normalized solid-state emission spectra of **[4-Ph(C^N^N)Pt]$_3$dpmp.** $\lambda_{ex} = 425$ nm.

In agreement with the discussion in the UV−vis absorption section, the metal−metal interactions are considered to be intramolecular rather than intermolecular not only because of the crystal structural evidence discussed earlier but also because of the two facts discovered from the solid-state emission and the emission in SDS (sodium *n*-dodecyl sulfate) micell solutions. As shown in Figure 7, the emission band maximum appears at 677 nm for the **[4-Ph(C^N^N)Pt]$_3$dpmp** powders and a film formed from a $\sim 10^{-4}$ mol/L CH_3CN solution after solvent evaporated, which is similar to the 700 nm band observed in solutions. The red shift of the emission band in solutions could be caused by the solvation effect. Because the 677 nm band is attributed to $^3[d\sigma^*, \pi^*]$ excited-state because of intramolecular metal−metal interactions, the emission band at 700 nm should arise from the intramolecular metal−metal interactions as well. The attribution of the 700 nm emission band to intramolecular rather than intermolecular metal−metal interaction is further supported by an emission study in SDS micell solutions, in which the concentration of SDS is adjusted to 1.4×10^{-2} mol/L. The SDS concentration surpasses the critical concentration required for the formation of micells and is at least 2 orders of magnitude higher than the **[4-Ph(C^N^N)Pt]$_3$dpmp** concentration added in the micell solution. In this case, each SDS micell can be considered as trapping only one **[4-Ph(C^N^N)Pt]$_3$dpmp** molecule. This eliminates the intermolecular interactions and prohibits the rotation along the oligophosphine axis. The emission observed in these micell solutions can thus be attributed to individual molecules. As shown in Figure 8, **[4-Ph(C^N^N)Pt]$_3$dpmp** in SDS micell solutions exhibits a dominant band at ~684 nm and a broad shoulder around 550 nm, which corresponds to the $^3[d\sigma^*, \pi^*]$ and ^{3}MLCT emission, respectively. The amount of **[4-Ph(C^N^N)Pt]$_3$dpmp** added into the micelle solution shows no effect on the emission spectra nor the relative intensity of the two emission bands. This further confirms that the 700 nm band in solution indeed arises from the intramolecular metal−metal interactions, not from the intermolecular interactions.

To confirm the hypothesis of conformational change caused by rotation of ligated Pt moiety along the oligophosphine axis, emission of 5.0×10^{-6} mol/L **[4-Ph(C^N^N)-**

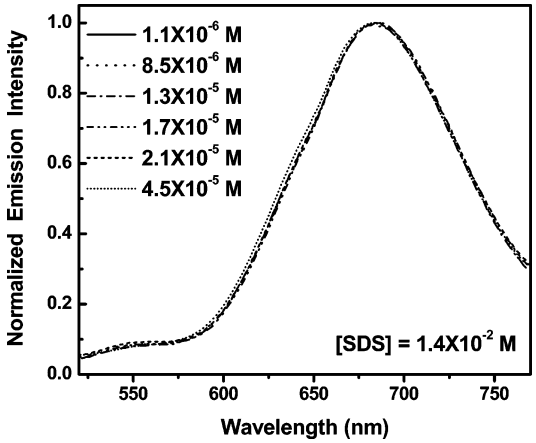

Figure 8. Normalized emission spectra of **[4-Ph(C^N^N)Pt]$_3$dpmp** in aqueous SDS micell solutions. [SDS] = 1.4×10^{-2} mol/L. $\lambda_{ex} = 400$ nm.

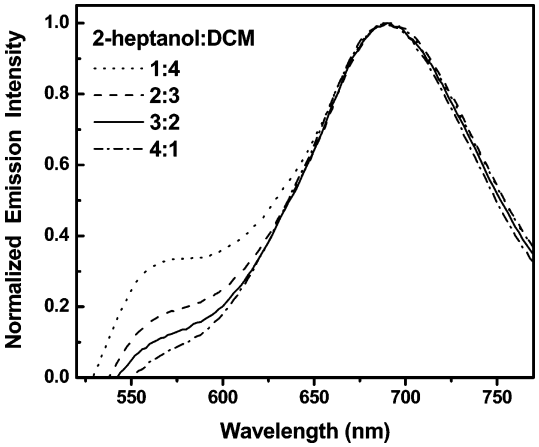

Figure 9. Normalized emission spectra of **[4-Ph(C^N^N)Pt]$_3$dpmp** in mixed solvents of 2-heptanol and dichloromethane. $\lambda_{ex} = 425$ nm.

Pt]$_3$dpmp solutions in mixed solvents with different viscosities has been studied, and the results are shown in Figure 9. 2-Heptanol and dichloromethane (DCM) were chosen as the solvents because they have the similar dielectric constants (9.21 for 2-heptanol and 8.93 for DCM) but quite different viscosities (6.53 for 2-heptanol and 0.45 for DCM). Therefore, the effect of solvent polarity can be excluded. The different emission behaviors observed in solutions with different volume ratios of these two solvents should arise from the difference in solvent viscosity and thus different degrees of rotation of the solute. It is clear from Figure 9 that in the mixed solvent with a lower viscosity, such as 2-heptanol/DCM = 1:4, rotation along the oligophosphine axis is relatively easier, thus the emission band around 550 nm due to mononuclear 4-Ph(C^N^N)Pt moiety is more intense. When the volume ratio of 2-heptanol increases, the viscosity of the mixed solvent increases and the rotation along the oligophosphine axis becomes less feasible. As a result, the amount of twisted conformers decreases, and the relative intensity of the 550 nm band decreases drastically. Excitation at different wavelengths, such as 380, 400, and 415 nm, gives rise to similar results. These results suggest that (1) the 700 nm band arises from intramolecular metal−metal interactions rather than intermolecular interactions because, if it is an intermolecular interaction, viscosity of solvent should not influence the relative emission intensity of the two bands and (2) conformational change caused by the rotation along the oligophosphine axis accounts for the relative intensity variation of the two emission bands and the degree of rotation is affected by the viscosity of the solvent. At low viscosity solvents, rotation is more feasible, the amount of twisted conformers increases. Therefore, the intensity of the 550 nm band increases.

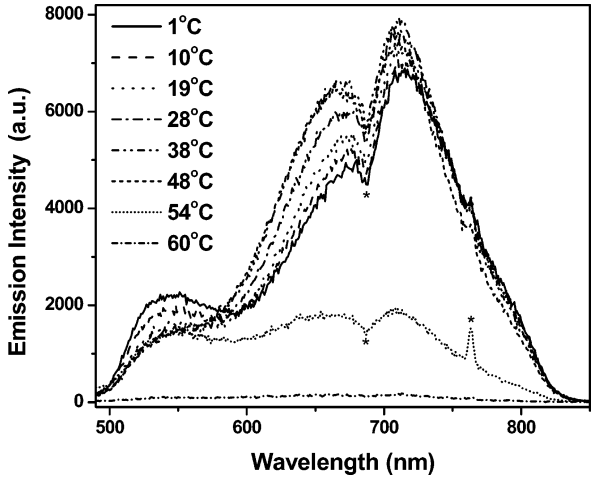

Figure 10. Temperature-dependent emission spectra of **[4-Ph(C^N^N)-Pt]$_3$dpmp** in CH_3CN at a concentration of 5.8×10^{-5} mol/L ($\lambda_{ex} = 380$ nm). The valley at 686 nm and the spike at 764 nm are instrument artifacts.

The temperature-dependent emission characteristics further supports this conformational transformation hypothesis. As shown in Figure 10, the emission at ∼542 nm decreases when the temperature increases from 1 to 38 °C, while the intensity of the emission band at ∼710 nm increases accompanied by a slight blue shift. When the temperature continues to increase, the intensity of the 542 nm band remains unchanged, but the low-energy band decreases rapidly. When the solution is heated to 60 °C, both emission bands disappear. This temperature-dependent behavior can be explained by the conformational change caused by rotation along the oligophosphine axis as discussed in the UV−vis absorption section and in the previous paragraph. When the temperature is increased from 1 to 38 °C, rotation along the oligophosphine ligand increases, resulting in more *syn* conformers. This leads to an enhancement of the $^3[d\sigma^*, \pi^*]$ emission. However, when the temperature continuously increases, the more rapid rotation reduces the Pt···Pt interactions, which decreases the intensity of the 710 nm band. At even higher temperatures, the enhanced nonradiative decays quench the emission from the **[4-Ph(C^N^N)Pt]$_3$dpmp** complex completely.

In addition to the evidence obtained from the temperature-dependent UV−vis absorption and emission studies, as well as the viscosity-dependent emission study, the temperature-dependent ^{1}H NMR spectra also indicate that there could be rotation to some extent along the oligophosphine ligand. As shown in Supporting Information Figure S3, at lower temperatures, the chemical shifts of the hydrogens on the coordinated pyridyl and phenyl rings appear at a relatively high field. With increased temperatures, the chemical shifts of the corresponding hydrogens shift to downfield. This

Table 4. Emission and Transient Absorption Lifetimes of **[4-Ph(C^N^N)Pt]$_3$dpmp** in Acetonitrile at Different Concentrations at Room Temperature and 77 K[a]

RT			77 K	
concentration ($\times 10^{-5}$ mol/L)	λ (nm) (τ_{em} (ns))	λ (nm) (τ_{TA} (ns))	concentration ($\times 10^{-5}$ mol/L)	λ (nm) (τ_{em} (ns, %))
0.08	550 (35)		0.7	573 (747, 13%; 39 419, 87%)
0.4	550 (52)	410 (49, 54%; 196, 46%); 600	2.1	712 (2882)
2	550 (59); 700 (81, 7%; 578, 93%)	410 (57, 27%; 386, 73%); 600 (61; 432)	6.3	715 (2642)
10	550 (84); 700 (708)	410 (73, 6%; 569, 94%); 600 (588)	18.8	712 (2655)
50	700 (944)		56.5	718 (2580)

[a] $\lambda_{ex} = 355$ nm.

phenomenon can be rationalized by the conformational change at different temperatures. At lower temperatures, the three ligated Pt(II) moieties tend to be arranged to a face-to-face conformation, as demonstrated by the crystal structure. Because of the short distance between the neighboring ligated Pt(II) moieties, the ring-current effect of the aromatic benzene and pyridine rings would cause the chemical shifts of the hydrogens on the aromatic rings at the other C^N^N ligand(s) appearing at upfield. When temperature increases, the rotation of the ligated Pt(II) moieties along oligophosphine ligand increases, the face-to-face arrangement of the three ligated Pt(II) moieties is destroyed, as a result, the electron-shielding effect decreases, and the chemical shifts of the corresponding hydrogens would shift to downfield. The line broadening and upfield shift were also observed by Yam and co-workers in some dinuclear platinum(II) terpyridine complexes with a flexible bridge and "sticky ends"[9d] and by Gourdon et. al. and Toma et. al. in some planar aromatic ruthenium complexes at low temperatures because of intramolecular/intermolecular metal−metal and $\pi-\pi$ stacking interactions.[14]

In addition to the downfield shift of the δ's at increased temperatures, the number of hydrogens corresponding to the most downfield peak (8.02 ppm) also changes. According to the estimation of ChemDraw software, the hydrogens at the 6/6′/6″-position (labeled in the structure shown in Figure 1) are the least shielded, and the hydrogens at 3/3′/3″ are the second least shielded in comparison to the other aromatic hydrogens. When the molecule adopts the face-to-face conformation, the hydrogens on 6/6″ positions of the peripheral coordinated pyridyl ring at the two edge-ligated Pt(II) moieties are less shielded compared to the corresponding hydrogen (6′) at the middle C^N^N moiety; therefore, the peak at the most downfield (8.02 ppm) should be assigned to these two hydrogens. The integration of this peak should correspond to two hydrogens. This is exactly the case at −30 °C. At high temperatures, such as 60 °C, because of the rotation of the three moieties along the oligophosphine ligand, the face-to-face conformation no longer exists, the hydrogens on the middle ligated Pt(II) moiety become less shielded. The chemical environment of 3,6-position hydrogens on all the three peripheral coordinated pyridyl rings thus becomes similar, resulting in an increase of hydrogen numbers (6H) corresponding to the most downfield peak (8.04 ppm).

The kinetic emission of **[4-Ph(C^N^N)Pt]$_3$dpmp** at different concentrations have been studied to determine the emission lifetime (see Supporting Information Figure S4 and S5 and Table 4). Similar to the steady-state emission spectra, emission of **[4-Ph(C^N^N)Pt]$_3$dpmp** at lower concentrations is dominated by the 550 nm band that has a lifetime of tens of nanoseconds. With increased concentrations, the relative intensity of this band gradually decreases, accompanied by the appearance of the 700 nm band that has a lifetime of hundreds of nanoseconds. When the concentration is increased to 5.0×10^{-4} mol/L, the high-energy band completely disappears. At 77 K, the emission is very weak at a low concentration of 7.0×10^{-6} mol/L, with a band maximum at 573 nm. From 2.1×10^{-5} to 5.7×10^{-4} mol/L, the glassy solutions exhibit only one emission band at ca. 710 nm, with a lifetime of approximately 2.6 μs.

It is worthy of mention that in comparison to the corresponding mononuclear complex **[4-Ph(C^N^N)Pt]PPh$_3$** ($\lambda_{em} = 550$ nm) and the dinuclear complex **[4-Ph(C^N^N)Pt]$_2$dppm** ($\lambda_{em} = 670$ nm), the emission energy of the trinuclear complex **[4-Ph(C^N^N)Pt]$_3$dpmp** ($\lambda_{em} = 700$ nm) decreases drastically, whereas the emission lifetime increases from 127 ns for **[4-Ph(C^N^N)Pt]PPh$_3$** to 202 ns for **[4-Ph(C^N^N)Pt]$_2$dppm**[6d] and to 944 ns for **[4-Ph(C^N^N)Pt]$_3$dpmp** in CH_3CN solutions. At a first glimpse, the decrease of emission energy and the increase of the emission lifetime seem to be associated with the metal−metal interactions that alter the parentage of the emitting state from ^{3}MLCT for mononuclear complex to ^{3}[dσ*, π*] for dinuclear and trinuclear complexes. The different emitting states could have different lifetimes. However, the longer lifetime of the dinuclear and trinuclear complexes could also possibly be caused by the block of the CH_3CN solvent access to the central 4-Ph(C^N^N)Pt component in the presence of the other 4-Ph(C^N^N)Pt component(s) above or below, which reduces the solvent quenching effect. To figure whether the reduction of solvent quenching or the metal−metal interaction accounts for the longer lifetime of the binuclear and trinuclear complexes, emission lifetimes of **[4-Ph(C^N^N)Pt]PPh$_3$**, **[4-Ph(C^N^N)Pt]$_2$dppm** and **[4-Ph(C^N^N)Pt]$_3$dpmp** at a concentration of $\sim 1 \times 10^{-4}$ mol/L were measured in a noncoordinating solvent DCM. The lifetimes were found to be 550 ns for **[4-Ph(C^N^N)Pt]PPh$_3$**, 1.3 μs for **[4-Ph-**

(14) (a) Gourdon, A.; Launay, J.-P. *Inorg. Chem.* **1998**, *37*, 5336. (b) Toma, S. H.; Uemi, M.; Nikolaou, S.; Tomazela, D. M.; Eberlin, M. N.; Toma, H. *Inorg. Chem.* **2004**, *43*, 3521.

(C^N^N)Pt]$_2$dppm, and 1.0 μs for **[4-Ph(C^N^N)Pt]$_3$dpmp.** Therefore, it is clear that the long-lived emission for **[4-Ph-(C^N^N)Pt]$_2$dppm** and **[4-Ph(C^N^N)Pt]$_3$dpmp** is caused by the nature of the ^{3}[dσ*, π*] excited-state that is further separated from the nonradiative d−d state in comparison to the high-lying ^{3}MLCT state. This reduces the nonradiative decay through d−d state and thus prolongs the lifetime of the ^{3}[dσ*, π*] state. Although the long-lived ^{3}[dσ*, π*] state could also possibly be caused by the different degrees of distortion of this state comparing to the ^{3}MLCT state, this possibility cannot be confirmed without theoretical calculations. Nevertheless, we believe the further separation of the ^{3}[dσ*, π*] state from the d−d state being the major cause based on the fact that some platinum complexes with a low-lying ^{3}MLCT state possess a long lifetime of approximately microseconds, which has been exemplified by our group for some platinum terpyridyl complexes with phenylacetylide ligand.[6b] The relatively shorter lifetime of **[4-Ph(C^N^N)-Pt]$_2$dppm** in CH_3CN should be attributed to the solvent quenching effect. To further demonstrate the effect of metal−metal interactions on the lifetime of the multinuclear system, mononuclear platinum triads with the open coordination sites blocked should be synthesized and studied in our future work.

Because of the charge-transfer nature of the emitting state, it is expected that both the emission energy and lifetime would be affected by the polarity of solvent. In contrast to the UV−vis absorption spectrum that exhibits a minimal and nonsystematic solvent-dependence, the emission energy, emission lifetime, and emission intensity all decrease pronouncedly when the polarity of the solvent increases (see Supporting Information Figure S6). This suggests that the ^{3}[dσ*, π*] state is more polar than that of the ground state. Polar solvents, such CH_3OH and CH_3CN, stabilize the polar excited-state more than the less polar ground state, which decreases the energy gap between the excited-state and the ground state, resulting in the red-shift of the emission band. As a consequence, the nonradiative decay rate increases, leading to the decrease of the emission intensity and the lifetime of the emission. A similar trend has been reported by Che and co-workers for the emission of a trinuclear platinum [{4,4′-^{t}Bu$_2$-(C^N^N)}$_3$Pt$_3$(μ_3-dpmp)](ClO$_4$)$_3$ complex.[9a]

Transient Absorption. It is well-known that the transient difference absorption measures the absorption difference between the excited-state and ground-state absorptions. If the excited-state absorption is stronger than that of the ground state at a given wavelength, a positive signal will appear. This phenomenon could lead to a reverse saturable absorption. To determine the spectral region for reverse saturable absorption, the transient difference absorption spectrum of **[4-Ph(C^N^N)Pt]$_3$dpmp** has been measured. As shown in Figure 11, the transient difference absorption spectrum of **[4-Ph(C^N^N)Pt]$_3$dpmp** exhibits two positive absorption bands, one at ~410 nm and the other at ~600 nm. In comparison to the corresponding mononuclear and dinuclear complexes, the positions of both bands red shift.[6d] The band at 410 nm exhibits a biexponential decay, with a short lifetime of 73 ns (6%) and a longer one of 569 ns (94%). In contrast, the 600 nm band exhibits a monoexponential decay

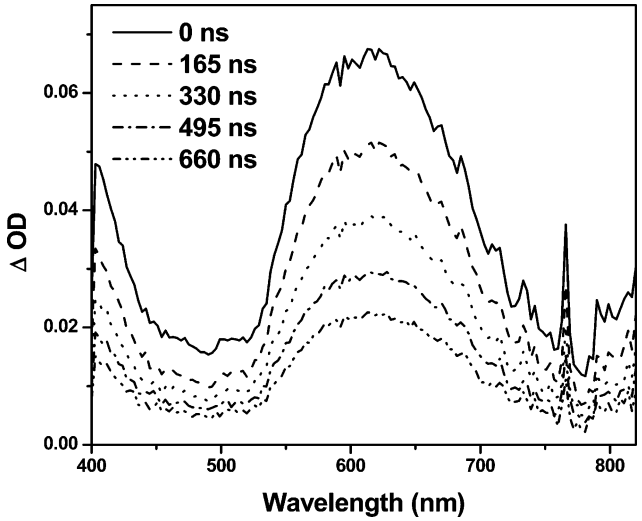

Figure 11. Time-resolved transient difference absorption spectra of **[4-Ph-(C^N^N)Pt]$_3$dpmp** in argon degassed CH_3CN at room temperature at a concentration of ~10^{-4} mol/L. λ_{ex} = 355 nm. The time listed in the figure is the time delay after the laser pulse.

with a lifetime of 588 ns. The similar excited-state lifetime obtained from the kinetic transient absorption measurement to that obtained from the kinetic emission measurement indicates that the transient absorption could arise from the same excited-state that emits or from a state that is in equilibrium with the emitting state. Therefore, the transient absorption could be attributed to the ^{3}[dσ*, π*] state, possibly mixed with some ^{3}MLCT character in view of the short-lived component of the 410 nm band.

As discussed in the emission section, because of the charge-transfer characteristic of the lowest excited state, the emission energy and lifetime are influenced by the polarity of solvent. Similar to the lifetime measured by the kinetic emission, the lifetime of the excited-state that gives rise to the transient absorption of **[4-Ph(C^N^N)Pt]$_3$dpmp** is also affected by the nature of the solvent. As presented in Table 3, the lifetime of **[4-Ph(C^N^N)Pt]$_3$dpmp** in more polar solvent (CH_3OH) is much shorter than those in less polar solvents (THF and DCM). This trend is consistent with what has been observed from the kinetic emission measurement. This further supports our assumption that the transient absorption state is the same as the emitting state, that is, the ^{3}[dσ*, π*] state.

Nonlinear Transmission. Because the transient absorption of **[4-Ph(C^N^N)Pt]$_3$dpmp** shows a broad, positive band from 500 to 750 nm and the lifetime of this band is hundreds of nanoseconds, it is expected that it would exhibit nonlinear transmission, namely, the transmission would decrease with increased laser energy at this spectral region. Surprisingly, the **[4-Ph(C^N^N)Pt]$_3$dpmp** CH_3CN solution with a linear transmission of 80% in a 2 mm thick quartz cell only exhibits negligible nonlinear transmission effect in the fluence region used in our experiment (shown in Figure 12). The nonlinear transmission behavior of the corresponding dinuclear platinum(II) complex **[4-Ph(C^N^N)Pt]$_3$dpmp** that exhibits comparable nonlinear transmission behavior to SiNc (a bench-

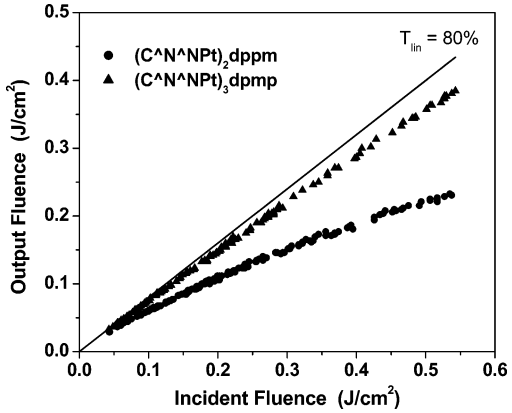

Figure 12. Incident fluence versus output fluence curves for the binuclear platinum(II) complex **[4-Ph(C^N^N)Pt]$_2$dppm** and trinuclear platinum(II) complex **[4-Ph(C^N^N)Pt]$_3$dpmp** for 4.1 ns laser pulses at 532 nm in a 2 mm cell. Both of these complexes were dissolved in acetonitrile. The linear transmission was adjusted to 80%.

mark nonlinear transmission material reported in literature)[15] has also been measured to evaluate the effect of metal−metal interactions on the nonlinear transmission behavior. It is very clear from Figure 12 that **[4-Ph(C^N^N)Pt]$_2$dppm** exhibits a much stronger nonlinear transmission than that of **[4-Ph(C^N^N)Pt]$_3$dpmp**. At the incident fluence of 0.53 J/cm^2, the transmittance of **[4-Ph(C^N^N)Pt]$_3$dpmp** decreases to 71%, while it decreases to 43% for **[4-Ph(C^N^N)Pt]$_2$dppm** at the same incident fluence. The nonlinear transmission threshold, defined as the incident fluence at which the transmittance drops to 90% of the linear transmittance, is found to be 0.45 J/cm^2 for **[4-Ph(C^N^N)Pt]$_3$dpmp** and lower than 0.04 J/cm^2 for **[4-Ph(C^N^N)Pt]$_2$dppm**. The much weaker nonlinear transmission of the trinuclear complex **[4-Ph(C^N^N)Pt]$_3$dpmp** could be attributed to its large ground-state absorption cross-section at 532 nm ($\sigma_0 = 1.8 \times 10^{-17}$ cm^2), which is nearly twenty times larger than that of **[4-Ph(C^N^N)Pt]$_2$dppm**.[6d] As has been pointed out in our previous work for the **[4-Ph(C^N^N)Pt]$_2$dppm** complex, the critical parameter that determines the degree of nonlinear transmission is the ratio of the excited-state absorption to ground-state absorption cross-section rather than the absolute value of the excited-state absorption cross-section.[6d] For the case of **[4-Ph(C^N^N)Pt]$_3$dpmp**, the enhanced intramolecular Pt···Pt interactions in comparison to those of the dinuclear complex **[4-Ph(C^N^N)Pt]$_3$dpmp** increases its ground-state absorption cross-section at 532 nm, which leads to a decrease of the ratio of the excited-state absorption cross-section to the ground-state absorption cross-section and in turn reduces the nonlinear transmission significantly.

To quantitatively compare the different ratio of excited-state absorption cross-section (σ_{eff}) to ground-state absorption cross-section (σ_0) for **[4-Ph(C^N^N)Pt]$_3$dpmp** and **[4-Ph(C^N^N)Pt]$_2$dppm**, the equation[16]

$$\sigma_{eff}/\sigma_0 = \ln T_{sat}/\ln T_{lin}$$

has been used, where T_{sat} is the transmittance at the saturation fluence (defined as $F_{sat} = h\nu/\sigma_0\Phi_t$, where Φ_t is the quantum yield of the first triplet excited state) and T_{lin} is the linear transmittance.

The σ_{eff}/σ_0 value was calculated to be 1.23 for **[4-Ph(C^N^N)Pt]$_3$dpmp** and 5.35 for **[4-Ph(C^N^N)Pt]$_2$dppm**. Although the nonlinear transmission of **[4-Ph(C^N^N)Pt]$_3$dpmp** at 532 nm is very weak, in view of the red shift of both the ^{1}[dσ*, π*] band in the UV−vis spectrum and the peak of the transient difference absorption spectrum, it is possible that the nonlinear transmission at longer wavelengths, such as 600 nm, could be stronger, which needs to be demonstrated in our future work.

Conclusion

The intramolecular Pt···Pt interactions in **[4-Ph(C^N^N)Pt]$_3$dpmp** lead to a broad and moderately strong absorption band from 400 to 600 nm, which is ascribed to the ^{1}[dσ*, π*] transition. These interactions also cause a red-shift of the emission band and transient difference absorption bands. The emission of this complex exhibits concentration, temperature, and viscosity dependence, indicating a conformational transformation. Because of the increased linear absorption cross-section at 532 nm, the nonlinear transmission of this complex at 532 nm is significantly reduced. However, with the strong and broad transient absorption band at ~600 nm and the long excited-state lifetime, this complex could possibly exhibit stronger nonlinear transmission at longer wavelengths, which may be confirmed in our future work.

Acknowledgment. Acknowledgement is made to the National Science Foundation (CAREER CHE-0449598) and Army Research Laboratory (W911NF-06-2-0032) for support. We also thank North Dakota State EPSCoR (ND EPSCoR Instrumental Award) for support. We are grateful to Dr. Hongshan He for his help in obtaining the crystal structure and the anonymous reviewers for valuable suggestions.

Supporting Information Available: Crystal data (CIF file), emission spectra at room temperature when excited at 491 nm, emission spectra at 77 K when excited at 530 nm, time-resolved emission spectra at different concentrations at room temperature and 77 K, emission spectra in different solvents at room temperature, and temperature-dependent ^{1}H NMR spectra in CD_3CN. This material is available free of charge via the Internet at http://pubs.acs.org.

IC700757X

(15) Mansour, K.; Alvarez, D., Jr.; Perry, K. J.; Choong, I.; Marden, S. R.; Perry, J. W. *Proc. SPIE—Int. Soc. Opt. Eng.* **1993**, *1853*, 132.

(16) Perry, J. W.; Mansour, K.; Marder, S. R.; Perry, K. J.; Alvarez, D., Jr.; Choong, I. *Opt. Lett.* **1994**, *19*, 625.